Global Research journal of Natural Science and Technology (Grjnst)
Volume: 03 - Issue 1 (2025)
p.ISSN: 2790-7643 e.ISSN: 2790-7651
www.grjnst.com

Visible-Light-Driven Photocatalytic Degradation of Ciprofloxacin Using Plasmonic Ag-Cu@SiO_2 Nanocomposites: Synergistic Effects and Mechanistic Insights

Iqra Ramzan
Faculty of Sciences, Superior University Lahore, Lahore 54000, Pakistan
Maryam Imbeisat
Institute of Chemistry, University of Sargodha, Sargodha 40100, Pakistan
Muhammad Ashraf Shaheen (Corresponding Author)
Faculty of Sciences, Superior University Lahore, Lahore 54000, Pakistan
Email: masaheen1964@gmail.com
Muhammad Azhar Abbas
Institute of Chemistry, University of Sargodha, Sargodha 40100, Pakistan/ Government Ambala Muslim Graduate College, Sargodha 40100, Pakistan

Abstract

The persistent release of antibiotic residues to water bodies has escalated antimicrobial resistance thus necessitating effective and viable cleanup technologies. This paper presents the synthesis and systematic assessment of a visible-light-responsive bimetallic Ag-Cu@SiO_2 photocatalyst in degrading ciprofloxacin (CIP) in water. Mesoporous silica support facilitated a uniform dispersion of the Ag-Cu nanoparticles, contributing to surface stability, light absorbing properties and reusability. Photocatalytic experiments showed the rapid and efficient CIP degradation in the presence of visible light and the degradation kinetics could be well explained by a pseudo-first-order model in the temperature range of 303 to 333 K with a low activation energy (8.67 kJ mol^{-1}) and a positive enthalpy which means the degradation process is energetically efficient. Radical scavenging experiments have verified that the major reactive species were superoxide radicals (O^{2-}) and photogenerated holes, and that the

minor role was played by hydroxyl radicals. It was found that the increased photocatalytic activity was due to the synergistic interaction of Ag-induced surface plasmon resonance and Cu-mediated charge separation that was efficient in preventing the electron-hole recombination. The reusability and stability of this catalyst were excellent since it retained its activity (more than 90 percent) in 5 consecutive cycles. All in all, Ag-Cu@SiO_2 photocatalyst has a high potential to be utilized practically in the treatment of antibiotic-contaminated wastewater under environmentally friendly conditions**.**

Keywords: Ag-Cu@SiO_2 photocatalyst, ciprofloxacin degradation, visible-light photocatalysis, plasmonic synergy, antibiotic wastewater treatment

1. Introduction

The prolonged release of antibiotics by hospitals, pharmaceutical industries, livestock farms, and domestic effluents has led to the accumulation of the bacterial agents in the water bodies (Bansal, 2019). Current surveys(UNEP, 2024) have shown that over fifty percent of the world river systems have been found to possess highest amounts of antibiotics that are beyond ecological safety levels (Wang et al., 2024). In 2024, World Health Organization (WHO) reported that, this contamination has caused an increase in the rate of antimicrobial resistance (AMR), which is predicted to have become a primary global threat, causing as many as 10 million deaths each year by 2050 (Ali et al., 2022a-c, 2023a-d, 2024, 2025, Hussain et al., 2021a, b; 2022, 2023, 2025a-c; Khatoon et al., 2025, Amjad et al., 2025; Shehzad et al., 2025; Iqbal et al., 2025; Rehman et al., 2025; Bisaccia et al., 2025; Salam et al., 2023). Thus, the invention of effective methods of antibiotic elimination has turned into a new pressing environmental concern (Muteeb et al., 2023).

Traditional methods of wastewater treatment like coagulation, biological filtration and chlorination have not been very effective in removing intractable antibiotics (Sangamnere et al., 2023; Umar, 2022). A large number of antibiotics are poorly biodegraded and highly chemically stable, which results in their leakage into effluents despite tertiary treatment (EPA, 2024) (Boro et al., 2025) (Ali et al., . In addition, chlorination produces poisonous

chlorinated products, whereas adsorption only transfers pollutants out of water to the solid matrices but does not totally degrade them (Gopal et al., 2007; Sun et al., 2023). These disadvantages illustrate the need to have a superior, catalytic degradation strategy. Photocatalysis has emerged as a promising oxidation technique, as exposure to visible light leads to the generation of highly reactive oxygen species (ROS), enabling the complete degradation of antibiotic contaminants rather than their mere phase transfer (Ashraf et al., 2022; Chen et al., 2022).

Bi-metallic photocatalysts, especially silver-copper (Ag-Cu) are the ones that exhibit better catalytic activity with synergistic effects between the two metals (Hao et al., 2024). Silver nanoparticles have a high surface plasmon resonance which enhances the absorption of visible-light, and copper components are used to trap electrons, inhibiting the recombination of charges (Sarina et al., 2013). This mixed alloy makes it thus more photo-oxidation efficient, and at the same time less dependent on expensive noble metals (Li et al., 2018).

Ag-Cu nanoparticles on silica do not only stop agglomeration of the particles, but also allow large surface area and stability to enhance photocatalytic activity with long term reuse (Habeche et al., 2023; Saran et al., 2018). SiO_2 mesoporous structure facilitates even dispersion of metal nanoparticles to increase the active redox sites (Kankala et al., 2019). The functionalization of Ag-Cu nano-particles onto silica support offers a structurally stable platform, which prefers to permit guided distribution and physical stabilization of the bimetallic assembly (Chang, 2020). The mesoporous SiO_2 network serves as an inert host network, which provides interconnected pores that take metal nanoparticles without exposing their surfaces to the reaction medium (Kankala et al., 2020; Kankala et al., 2019). This confinement in structure helps in maintaining the stability of the particles during irradiation and aqueous conditions thus maintaining stable catalytic behavior during repeated photocatalytic cycles (Shchukin & Sviridov, 2006; Y. Zhang et al., 2025). In addition, silica is highly porous, making it more passive to diffusion of dissolved oxygen and pollutants of dissolved molecules to the metal-active sites, which is a requirement of surface-mediated redox reactions (Z. Zhang et al., 2025). Though, Since $SiO_2$is not directly involved in photoactivity, its use in the form of a dispersing and stabilizing support indirectly enhances the performance and stability of the Ag-Cu photocatalyst (Babu & Naik, 2020).

This paper therefore attempts to prepare an immensely efficient bimetallic Ag-Cu on silica photocatalyst to degrade antibiotics using visible light. Alloy composition, light response and reusability were systematically considered to determine its practical application by purifying wastewater.

2. Materials and Methods

2.1. Chemicals

Silver nitrate ($AgNO_3$, 99%), copper sulfate pentahydrate ($CuSO_4.5H_2O$, 98%), and tetraethyl orthosilicate (TEOS, 98%) are these and are obtained at Sigma-Aldrich. $NaBH_4$ (>98%), ethanol (99.5%), hydrochloric acid (HCl, 0.1 M) and sodium hydroxide (NaOH) were purchased at Merck. The antibiotic pollutant (ciprofloxacin) that was selected to apply in photocatalysis was acquired through Sigma-Aldrich. Without further purification, all of the analytical-grade chemicals were used, and deionized (DI) water was used in all experiments.

2.2. Synthesis of Ag-Cu Supported on Silica Synthesis

2.2.1. Silica Support Synthesis

Synthesis of silica support was done using a standard sol gel pathway (Li et al., 2005). In short, TEOS, ethanol and DI water were added to each other in 1:4:4 volumetric proportion after which dilute HCl was added to achieve an acidic pH of approximately 2. Silanol intermediates were produced as a result of the hydrolysis of TEOS in the acidic environment. The stirring mixture was kept at the room temperature during 1 hour, which led to sol-gel conversion and the appearance of a clear gel. The gel was left to develop at room temperature of 12-24 hours in order to consolidate the silica network, and then it was carefully washed with ethanol and DI water in order to wash out any unreacted precursors. The material obtained was dried at 80 °C overnight and then calcined at a temperature of 450-500 °C, 3 hours to obtain an aerated, thermally stable silica support.

2.2.2. Ag-Cu Nanoparticles Impregnation and Reduction on Silica

The wet impregnation technique was used to incorporate bimetallic Ag-Cu nanoparticles onto silica. $AgNO_3$ and $CuSO_4$ were dissolved separately in aqueous solutions and combined to

achieve the required molar Ag-Cu ratio (1:1, 1:3 or 3:1). The support of calcified silica was dispersed into the mixed metal solution and ultrasonicated in 30 minutes and thereafter the mixture was stirred continued stirring of 4-6 hours to ascertain that the metal ions were adsorbed on the surface of silica. The mixture was then dried at 7080 o C to produce metal-laden silica powder. Reducing metal ions (Ag^+ and Cu^{2+}) to alloy nanoparticles was done by dropwise addition of freshly prepared 0.1 M $NaBH_4$ under steady stirring in an ice bath to prevent uncontrolled nucleation. The catalyst was then filtered, rinsed with ethanol and DI water, and dried at 60 to 70 °C. Thermal reduction was used in another reduction method where the impregnated silica was heated in tube furnace at the presence of N_2 at 350 °C for 2-3 hours which allowed the formation of Ag^0-Cu^0 alloy nanoparticles.

2.3. Photocatalytic Activity

Photocatalytic performance of the synthesized Ag-Cu@SiO_2 catalyst was assessed by the degradation of CIP in aqueous solution under irradiation of visible light. A common experiment entailed the dispersal of a known concentration of photocatalyst in a CIP solution of specified initial concentration and magnetic stirring at the dark stage of 30 min to achieve adsorption desorption equilibrium. The suspension was then subjected to visible light by keeping the suspension in constant motion so as to have a uniform irradiation. Aliquots were sampled at intervals and centrifuged to clear the catalyst followed by the determination of the remaining CIP concentration by the use of UV-vis spectrophotometry at the wavelength at which it showed its characteristic absorption intensity. The change in the absorbance divided by the original value was taken to determine the degradation efficiency (Ma et al., 2023). The dosage of the catalyst, solution pH, irradiation time, temperature, and reusability of the catalyst were investigated systematically under the same experimental conditions to determine the feasibility of photocatalytic practicality of the A-gCu@SiO_2 catalyst.

3. Application

3.1. Photocatalytic Degradation

Photocatalytic activity of Ag-Cu@SiO_2 supported on silica was tested to degrade CIP, a common fluoroquinolone antibiotic and a gradually emerging water pollutant. Taking into

account the high impact of the environmental factors on the photocatalytic activity, the experiments were carried out under the conditions of the controlled light irradiation of the catalyst to determine the practical applicability of the catalyst to the environmental remediation. Figure 1A shows the UV- Vis absorption spectrum of CIP through constant intervals of irradiation with an observation that the typical absorption peaks of the antibiotic decreases gradually. The percent (%) of degradation efficiency of CIP was determined using Equation 1.

$$Degradation\ efficiency\ (\%) = \frac{A_0 - A_t}{A_0} \times 100 \qquad (1)$$

In which A_0 is the initial absorbance and A_t absorbance at time t, respectively. Figure 1(B) indicates the percentage of photocatalytic degradation of CIP as a function of the irradiation time. The findings indicate that the Ag-Cu@SiO_2 catalyst has a significant photocatalytic rate, resulting into a good degradation rate of CIP in the reaction time studied. In determining the feasibility of the reusability of the catalyst in practice, experiments on degradation were carried out in several consecutive cycles under the same conditions of the reaction. The catalyst also showed a high degree of stability and deactivation resistance which means that it maintained a large fraction of its photocatalytic activity in consecutive cycles. Moreover, the dosage of catalyst on the CIP degradation was studied through different concentrations of Ag-Cu@SiO_2. The rate of degradation was found to increase with the increasing quantity of catalyst to an optimal point, beyond which, the rate of degradation decreased. One can explain this decrease in higher doses of catalysts by the fact that the reaction medium becomes very turbid, which inhibits penetration of light and causes photons to be less available in order to be activated by photocatalysts. The reaction medium pH is also a determining factor in the process of photocatalytic degradation because it influences the charge of the catalyst on the surface and the ionic state of CIP molecules. The degradation characteristic of CIP at various pH values is shown in the figure below. The findings reveal that the pH of a solution plays an important role in determining the photocatalytic behavior because electrostatic interactions of the catalyst surface and antibiotic molecules are different in relation to the pH of the solution. Altogether, the Ag-Cu@SiO_2 photocatalyst has a high

potential of the degradation of CIP, which supports its suitability in the treatment of the antibiotic-contaminated water.

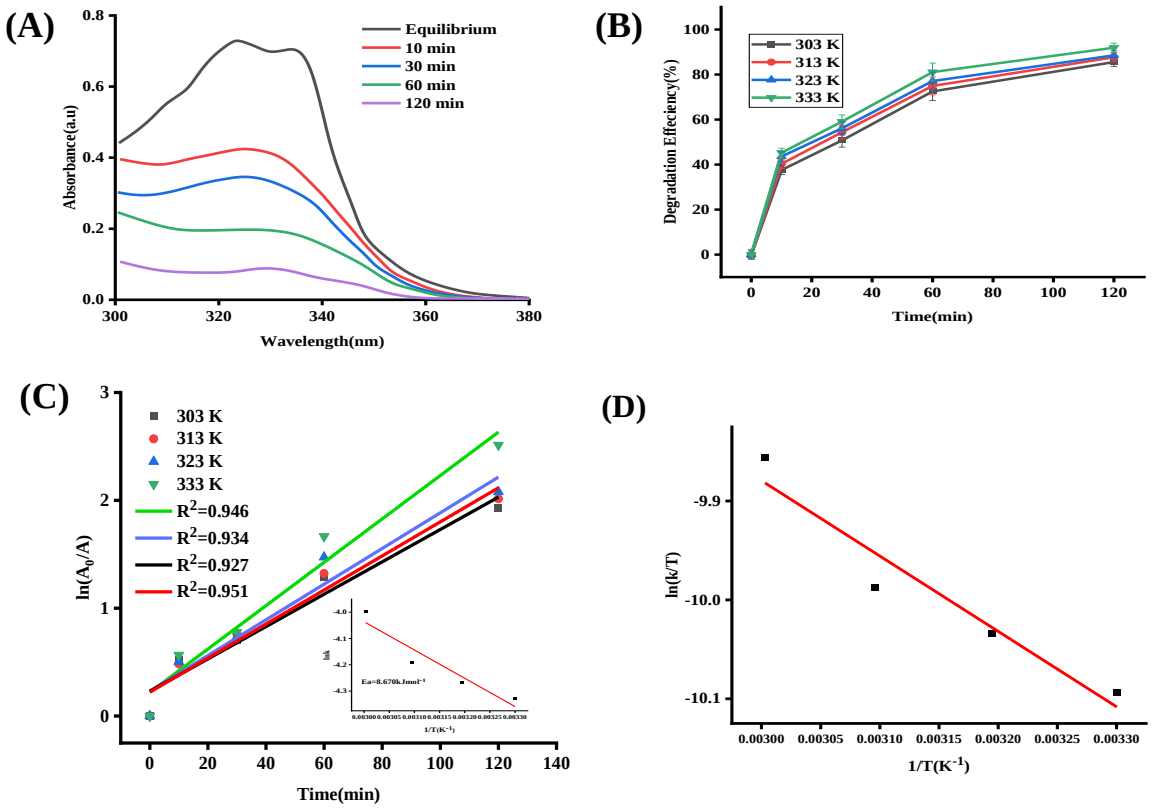

Fig.1 (A) UV-vis absorption spectra of CIP during photocatalytic degradation using Ag-Cu@SiO_2 catalyst, (B) degradation efficiency as a function of irradiation time, (C) pseudo-first-order kinetic plots for CIP degradation, and (D) linear fitting of the kinetic model.

3.2. Kinetics of CIP Degradation

The photocatalytic decomposition of CIP was studied under four temperatures (303, 313, 323 and 333 K) with constant irradiation time. In order to explain the degradation kinetics of CIP, the absorbance of the material at a characteristic wavelength was observed vs irradiation time. The apparent rate constant (k) was calculated by using a pseudo-first-order kinetic model based on the equation below:

$$ln(A_0 / A_t) = kt \qquad (2)$$

In which A_0 and A_t are the absorbance of CIP at time 0 and time t, respectively, and k is the apparent rate constant of the photocatalytic degradation reaction. Fig. 1(C) demonstrates the plots of ln (A_0/At) versus the irradiation time of CIP degradation at various temperatures and the rate constants (k) were obtained by the slope of the linear fitted lines. The values of the rate constant of the CIP degradation at the studied temperatures are summarized in Table 1. The fact that the experimental data were well fitted by the good line supports the fact that the photocatalytic degradation of CIP is governed by the pseudo-first-order model of kinetics. Moreover, the linear regression coefficients (R^2) were also known to be approaching unity at all the temperatures studied and thus, there was a perfect agreement between experimental results and kinetic model. This finding also confirms the hypothesis that CIP reduction on the Ag-Cu@SiO_2 catalyst occurs through pseudo-first-order kinetics. Besides, the effect of the initial CIP concentration and the existence of other coexisting ions on the rate of degradation was also investigated. It was noted that the degradation efficiency of the initial CIP concentration decreased as the initial CIP concentration increased and this could be explained by the diminished availability of active surface sites per antibiotic molecule and the partial absorption of incident light by CIP molecules at higher concentration. Besides, the slowing down of the degradation rate constant in the presence of carbonate and chloride ions can be linked to the scavenging activity of these ions on reactive oxygen species, especially the hydroxyl radicals.

3.3. Thermodynamics Parameters

To measure the activation energy (Ea) and thermodynamic parameters, such as enthalpy change (ΔH), entropy change (ΔS) and Gibbs free energy change (ΔG), the photocatalytic degradation of CIP was studied at four temperatures (303, 313, 323, and 333 K). The Arrhenius equation was applied to calculate the activation energy:

$$ln\, k = -\frac{E_a}{RT} + ln\, A_t \qquad (3)$$

and k is the degradation reaction rate constant, A is an Arrhenius pre-exponential factor, R is the universal gas constant (8.314 kJ mol^{-1}), and T is the absolute temperature. The inset of

Fig. 1(C) gives the plot of lnk vs1/T. Ea was obtained by the slope of the lnk versus 1/T plot, and the slope value of Ea is =8.67kJmol^{-1} The Eyring Polanyi equation below was used to find enthalpy change of activation (ΔH) and entropy change of activation (ΔS).

$$ln\left(k/T\right) = -\Delta H/RT + \Delta S/R + \ln(k_B/h) \quad (4)$$

with k being the rate constant, and k_B, and h being the Boltzmann and the Planck constants respectively. Another linear correlation between ln(k/T) and 1/T was found as illustrated in Fig. 1(D). The slope and intercept of this plot were used to give the values of ΔH and ΔS, which are presented as ΔH is 6.030997kJ mol^{-1} and ΔS is -0.2614 kJ mol^{-1} K^{-1}, respectively. The following equation was used to calculate the Gibbs free energy change of activation

$$\Delta G = \Delta H - T\Delta S \quad (5)$$

Table 1 shows the results of the computations of ΔG in various temperatures. The rate constant (k), energy of activation (Ea) and thermodynamic (ΔH, ΔS and ΔG) of the values of these equations are listed in Table 1. As it can be seen, the larger the values of rate constants, the smaller the activation energy, and the faster the reaction with a lower energy barrier occurs (Phillips, 1992). The magnitude and value of ΔH show that the degradation of CIP by a specific reaction is of the nature of, whereas the value of ΔS indicates that the transition of states happens with a change of disorder, which is adiabatic. The positive values of ΔG are positive therefore the degradation process is under the researched conditions.

Table 1. Tthermodynamics parameters of degradation of CIP at Ag-Cu@SiO_2.

Temperature (K)	***k*** **(min^{-1})**	**E_a (kJ mol^{-1})**	**ΔH (kJ mol^{-1})**	**ΔS (kJ mol^{-1} K^{-1})**	**ΔG (kJ mol^{-1})**
303	0.013171				85.23
313	0.014025	8.674	6.030997	-0.2614	87.85
323	0.014705				90.46
333	0.018362				93.07

3.4. Regeneration of the Ag-Cu@SiO_2 Photocatalyst

The Ag-Cu@SiO_2 photocatalyst was demonstrated to be reusable in the degradation of CIP in several cycles. First, CIP was degraded using Ag-Cu@SiO_2 catalyst under the influence of visible light. Upon completion of every degradation cycle, the photocatalyst was centrifuged at 6000 rpm during 25 min. The supernatant that carried over CIP was discarded and the obtained catalyst to be recovered was washed three times using deionized water to take away any adsorbed residues. The resulting clean photocatalyst was dried in an oven at 60°C for 12 hours and reused to perform further CIP degradation cycles in the same experimental conditions. Unlike in Fig. 2A, the degradation efficiency of CIP reduced insignificantly with repeated usage. Five consecutive cycles still resulted in a slight decrease (around 10) in the photocatalytic activity suggesting that the Ag-Cu@SiO_2 catalyst is very stable and reusable. These findings indicate that Ag-Cu@SiO_2 is a promising candidate to be used in real-world wastewater treatment practice since this material can be successfully utilized to treat CIP on several cycles without notable catalytic decline.

3.5. Scavenging Activity

The degradation of organic contaminants is primarily caused by reactive oxygen species (ROS), such as hydroxyl radicals (•OH), superoxide anion radicals (O^{2-}), hydrogen peroxide (H_2O_2), and photogenerated holes (h^+) (Xie et al., 2022). In order to assess the role of individual reactive species in CIP degradation, a radical scavenging experiment was performed with the Ag-Cu@SiO_2 as the photocatalyst. Four scavengers were used, namely disodium ethylenediamine tetraacetate (Na 2 EDTA) as h^+, p -benzoquinone (p -BQ) as O^{2-}, isopropanol (IPA) as OH, and L-ascorbic acid (L -AA) as H_2O_2. A scavenger 0.2 mM was used in each experiment, which was added to a 10 ppm CIP solution, and 20 mg of Ag-Cu@SiO_2 catalyst was added. The decay of CIP was trailed under sun light by the above-described method. All scavengers inhibited the degradation of CIP as demonstrated in Fig. 2B, and this proved the occurrence of all the reactive species in the course of photocatalysis. It is worth noting that when p-BQ and Na_2EDTA were added, there was a strong inhibition of CIP removal hence indicating that the O^{2-} is the dominating factor and h^+ plays the secondary role in the degradation of CIP on the Ag-Cu@SiO_2 surface.

The bandgap of Ag-Cu@SiO_2 was valence band (VB) and conduction band (CB).

$$E_{CB} = X - E_C - 0.5E_g \qquad (6)$$

$$E_{VB} = E_{CB} + E_g \qquad (7)$$

Butler Ginley equations were used to determine the band edge positions of Ag-Cu@SiO_2 using E_{CB}= -1.34e and E_{VB}= +1.46e. The E_{CB} is a negative value that is negative enough toward thermodynamic favoring the formation of superoxide radical (O^{2-}), which agrees with the strong inhibition of pp-benzoquinone in the scavenger tests (Hayyan et al., 2016).

3.6. Photocatalytic Degradation Mechanism of CIP over Ag-Cu@SiO_2 Catalyst

The first step would be to activate the Ag-Cu@SiO_2 photo-catalyst by the absorption of light energy of UV, visible or sunlight. This is the energy of light that must not be less than equal to the band gap of the photo-catalyst (Tantawy et al., 2021). Consequently, electrons in the valence band get excited and shift to the conduction band leaving a hole in the valence band. It is in this process that the degradation reaction is initiated and that is given by equation

$$Ag-Cu@SiO_2 + hv \rightarrow Ag-Cu@SiO_2 + \left[e^-(CB) + h^+(VB)\right] \qquad (8)$$

Upon light irradiation, the Ag-Cu@SiO_2 photocatalyst is activated, causing electrons to be excited from the valence band to the conduction band and leaving behind positively charged holes. The photogenerated electrons are readily captured by dissolved oxygen molecules, leading to the formation of superoxide radical species(Lupano et al., 2013) .

$$O_2 + e^-(CB) \rightarrow^{\bullet} O_2^- \qquad (9)$$

Simultaneously, the photogenerated holes exhibit strong oxidative capability and react with water molecules or hydroxyl ions adsorbed on the catalyst surface, resulting in the generation of highly reactive hydroxyl radicals.

$$H_2O + h^+(VB^+) \rightarrow^{\bullet} OH + H^+ \qquad (10)$$

$$OH^- + h^+(VB) \rightarrow^{\bullet} OH \qquad (11)$$

The superoxide radicals produced further participate in a series of chain reactions. In the presence of protons, superoxide radicals are converted into hydroperoxyl radicals, which subsequently combine to form hydrogen peroxide.

$$^{\bullet}O_2 + H^+ \rightarrow HOO^{\bullet} \quad (12)$$

$$2HOO^{\bullet} \rightarrow H_2O_2 + O_2 \quad (13)$$

The hydrogen peroxide generated in the system is further reduced by conduction band electrons, producing additional hydroxyl radicals and thus sustaining the oxidation process.

$$H_2O_2 + e^- \rightarrow {}^{\bullet}OH + OH^- \quad (14)$$

The presence of bimetallic Ag-Cu nanoparticles significantly enhances the photocatalytic process (Ismail et al., 2018). Silver nanoparticles generate additional electrons through surface plasmon resonance under light irradiation, while copper ions act as efficient electron acceptors, thereby suppressing electron-hole recombination.

$$Ag^0 + h\nu \rightarrow Ag^+ + e^- \quad (15)$$

$$Cu^{2+} + e^- \rightarrow Cu^+ \quad (16)$$

$$Cu^+ + O_2 \rightarrow Cu^{2+} + {}^{\bullet}O_2^- \quad (17)$$

The reactive oxygen species generated in the system attack CIP molecules through multiple pathways. Hydroxyl radicals preferentially attack the piperazine ring, leading to hydroxylation followed by ring opening.

$$CIP + {}^{\bullet}OH \rightarrow Hydroxylated\ intermediate \quad (18)$$

In parallel, the quinolone core of CIP undergoes direct oxidation by valence band holes, resulting in the breakdown of the aromatic structure.

$$CIP + h^+(VB) \rightarrow Oxidation products \quad (19)$$

Defluorination also occurs during the degradation process, where hydroxyl radicals cleave the C–F bond, contributing to detoxification of the antibiotic molecule.

$$C-Fbond+^{\bullet}OH \rightarrow HF+Hydxylatedproduct \qquad (20)$$

Additionally, CIP molecules can directly accept electrons from the conduction band, forming reduced intermediates that are more susceptible to further oxidation.

$$CIP+e^{-}(CB) \rightarrow \mathrm{Re}duced\ \mathrm{int}ermediate \qquad (21)$$

Through continuous attack by reactive oxygen species and photogenerated charge carriers, the resulting intermediates are progressively oxidized and ultimately mineralized into simple and environmentally benign products.

$$C_{17}H_{18}FN_3O_3+37^{\bullet}OH \rightarrow 17CO_2+HF+NH_4+NO_3^{-}+15H_2O \qquad (22)$$

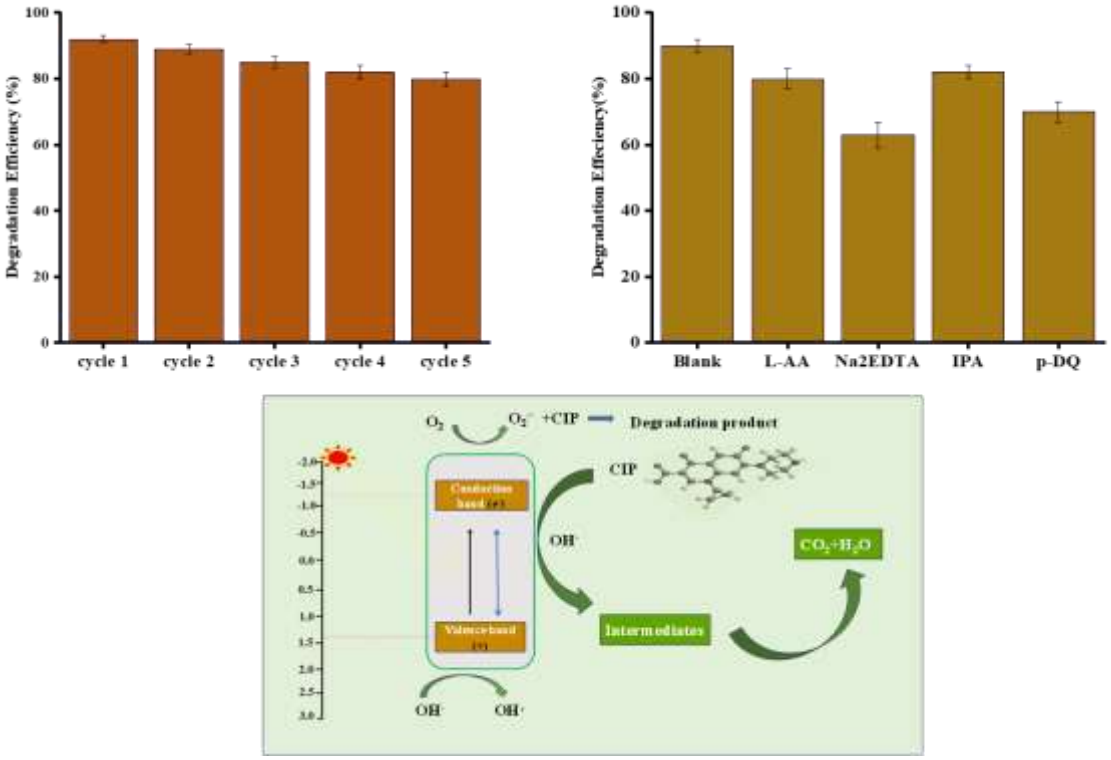

Fig 2. (A) Regeneration results show the efficiency of the Ag-Cu@SiO_2 photocatalyst for CIP degradation after five consecutive cycles. (B) Degradation efficiency of different

radicals. (C) Schematic illustration of the photocatalytic degradation mechanism of Ag-Cu@SiO_2 for CIP antibiotic.

4. Conclusion

This research shows that a rational design of a bimetallic Ag-Cu @SiO_2 photocatalyst allows a high performance and stability in degrading CIP under visible-light irradiation. The biosensing synergistic interaction between Ag and Cu nanoparticles, grown on mesoporous silica, significantly enhances light harvesting, charge separation, and catalyst deactivation resistance. The degradation was under pseudo-first-order kinetics and with low activation energy, and this was a confirmation that there is a kinetically and energetically favored process. Mechanistic studies showed that the oxidation pathway is controlled by superoxide radicals and holes generated by photochemical reaction whereas hydroxyl radicals mediate the stepwise degradation, defluorination and mineralization of CIP. Notably, the catalyst was highly active in various reuse cycles, and this shows the operational strength of the catalyst. These results put Ag-Cu@SiO_2 as a cost effective and environmentally friendly photocatalyst in the real-world treatment of antibiotic contaminated wastewater**.**

References

Ashraf, A., Liu, G., Yousaf, B., Arif, M., Ahmed, R., Rashid, A., Riaz, L., & Rashid, M. S. (2022). Phyto-mediated photocatalysis: a critical review of in-depth base to reactive radical generation for erythromycin degradation. Environmental Science and Pollution Research, 29(22), 32513-32544.

Ali, A., Akram, A., Bakar, M.A., Amin, H.M., Zohra, L., Abbas, A., Sher, M., Hussain, M.A., Haseeb, M.T. & Imran, M. (2025). A model batch and column study for Cd (II) uptake using citric acid cross-linked *Salvia spinosa* hydrogel: Optimization through Box-Behnken design. Journal of Industrial and Engineering Chemistry, 151, 746-761.

Hussain, A., Fatima, S., Abbas, A., Ali, A., Amin, M., Muhammad, G. & Sher, M. (2023). Removal of Cr (III) and Ni (II) from aqueous solution using a mixed cellulose ether-ester hydroxyethylcellulose adipate. Desalination and Water Treatment, 283, 153-163.

Hussain, M.A., Gul, S., Abbas, A., Ali, A. & Alotaibi, N.F. (2021a). Chemically modified rhamnogalacturonans from linseed: a supersorbent for Cd^{2+} and Pb^{2+} uptake from aqueous solution. Desalination and Water Treatment, 221, 163-175.

Shehzad, M.K., Ali, A., Qasim, S., Mumtaz, A., Hussain, M.A., Fawy, K.F., Nishan, U., Azhar, I., Abbas, M.A. & Abba, A. (2025). Sustainable remediation of cadmium using succinate-functionalized glucoxylan from chia (*Salvia hispanica*) seeds hydrogel. Journal of Industrial and Engineering Chemistry. https://doi.org/10.1016/j.jiec.2025.10.034

Ali, A., Haseeb, M.T., Hussain, M.A., Tulain, U.R., Muhammad, G., Azhar, I., Hussain, S.Z., Hussain, I. & Ahmad, N. (2023a). A pH responsive and superporous biocomposite hydrogel of *Salvia spinosa* polysaccharide-co-methacrylic acid for intelligent drug delivery. RSC Advances, 13(8), 4932-4948.

Ali, A., Hussain, M.A., Haseeb, M.T., Farid-Ul-Haq, M., Erum, A. & Hussain, M. (2024). Acute toxicity studies of methacrylic acid based composite hydrogel of *Salvia spinosa* seed mucilage: a potential non-toxic candidate for drug delivery. Cellulose Chemistry and Technology, 58(1-2), 45-53.

Ali, A., Hussain, M.A., Haseeb, M.T., Tulain, U.R., Farid-ul-Haq, M., Tabassum, T., Muhammad, G., Hussain, S.Z., Hussain, I. & Erum, A. (2023b). Synthesis, characterization, and acute toxicity of pH-responsive *Salvia spinosa* mucilage-co-acrylic acid hydrogel: A smart excipient for drug release applications. Reactive and Functional Polymers, 182, 105466.

Ali, A., Hussain, M.A., Abbas, A., Khan, T.A., Muhammad, G., Haseeb, M.T. & Azhar, I., (2022a). Comparative isoconversional thermal analysis and degradation kinetics of *Salvia spinosa* (Kanocha) seed hydrogel and its acetates: a potential matrix for sustained drug release. Cellulose Chemistry and Technology, 56(3-4), 239-250.

Ali, A., Hussain, M.A., Haseeb, M.T., Ashraf, M.U., Farid-ul-Haq, M., Tabassum, T., Muhammad, G. & Abbas, A. (2023c). pH-responsive, hemocompatible, and non-toxic polysaccharide-based hydrogel from seeds of *Salvia spinosa* L. for sustained release of febuxostat. Journal of the Brazilian Chemical Society, 34, 906-917.

Rehman, A.U., Maqsood, A., Siddique, A.B., Akhtar, S., Fawy, K.F., Ain, Q.U., Sher, M., Nishan, U., Ahmad, T., Ali, A. & Abbas, A. (2025). From waste to water treatment: Banana peel powder for polystyrene removal with FTIR-based mechanistic understanding. Journal of Industrial and Engineering Chemistry. https://doi.org/10.1016/j.jiec.2025.11.036

Ali, A., Hussain, M.A., Haseeb, M.T., Bukhari, S.N.A., Tabassum, T., Farid-ul-Haq, M. & Sheikh, F.A. (2022b). A pH-responsive, biocompatible, and non-toxic citric acid cross-linked polysaccharide-based hydrogel from *Salvia spinosa* L. offering zero-order drug release. Journal of Drug Delivery Science and Technology, 69, 103144.

Amjad, F., Ali, A., Hussain, M.A., Haseeb, M.T., Ajaz, I., Farid-ul-Haq, M., Hussain, S. Z. & Hussain, I. (2025). A superabsorbent and pH-responsive copolymer-hydrogel based on glucomannans from *Ocimum basilicum* (sweet basil): A smart and non-toxic material for intelligent drug delivery. International Journal of Biological Macromolecules, 315(2), 144452.

Ali, A., Haseeb, M.T., Hussain, M.A., Muhammad, T., Muhammad, G., Ahmad, N., Alotaibi, N.F., Hussain, S.Z. & Hussain, I. (2022c). Extraction optimization of a superporous polysaccharide-based mucilage from *Salvia spinosa* L. Cellulose Chemistry and Technology, 56, 957-969.

Iqbal, J., Kanwal, M., Siddique, A., Fawy, K.F., Sher, M., Nishan, U., ur Rehman, M.F., Abbas, M.A., Ali, A. & Abbas, A. (2025). β-Cyclodextrin-functionalized silver nanoparticles as a visual probe for selective tetrahydrocannabinol detection via host–guest induced plasmonic shifts. Microchemical Journal, 116177.

Hussain, M.A., Shahzad, K., Ali, A., Haseeb, M.T. & Hussain, S.Z. (2025a). Development of a novel smart bio-composite hydrogel based on dextran, citric acid, and glucoxylan for pH-dependent drug delivery and stimuli-responsive swelling and release. Polymers and Polymer Composites, 33, p.09673911251350240.

Khatoon, M., Ali, A., Hussain, M.A., Haseeb, M.T., Muhammad, G., Sher, M., Hussain, S.Z., Hussain, I. & Iqbal, M. (2025). A chia (*Salvia hispanica* L.) seed mucilage-based glucoxylan-grafted-acrylic acid hydrogel: a smart material for pH-responsive drug delivery systems. Materials Advances, 6(8), 2636-2647.

Hussain, M.A., Raees, N., Ali, A., Tayyab, M., Muhammd, G., Uroos, M. & Batool, M., (2025b). Optimization of rhamnogalacturonan extraction from linseed using RSM and designing a pH-responsive tablet formulation for sustained release of ciprofloxacin. Cellulose Chemistry and Technology, 59, 547-558.

Hussain, M.A., Taj, T., Ali, A., Haseeb, M.T., Hussain, S.Z., Muhammad, G. & Bukhari, S.N.A. (2025c). Cross-Linking of Hydroxypropylcellulose With Flaxseed Rhamnogalacturonans Using Citric Acid Produces a Hemocompatible Biocomposite for pH-Responsive Rifaximin Delivery. Journal of Applied Polymer Science, e57486.

Hussain, M.A., Abbas, A., Yameen, E., Ali, A., Muhammad, G., Hussain, M. & Shafiq, Z., (2022). Adsorptive removal of Pb^{2+} and Cu^{2+} from aqueous solution using an acid modified glucuronoxylan-based adsorbent. Desalination and Water Treatment, 248, 163-175.

Hussain, M.A., Abbas, A., Habib, M.G., Ali, A., Farid-ul-Haq, M., Hussain, M., Shafiq, Z. & Irfan, M.I. (2021b). Adsorptive removal of Ni (II) and Co (II) from aqueous solution using succinate-bonded polysaccharide isolated from Artemisia vulgaris seed mucilage. Desalination and Water Treatment, 231, 182-195.

Ali, A., Hussain, M.A., Abbas, A., Haseeb, M.T., Azhar, I., Muhammad, G., Hussain, S.Z., Hussain, I. & Alotaibi, N.F. (2023). Succinylated *Salvia spinosa* hydrogel: Modification, characterization, cadmium-uptake from spiked high-hardness groundwater and statistical analysis of sorption data. Journal of Molecular Liquids, 376, 121438.

Babu, P., & Naik, B. (2020). Cu–Ag bimetal alloy decorated SiO2@ TiO2 hybrid photocatalyst for enhanced H2 evolution and phenol oxidation under visible light. Inorganic Chemistry, 59(15), 10824-10834.

Bansal, O. (2019). Antibiotics in hospital effluents and their impact on the antibiotics resistant bacteria and remediation of the antibiotics: a review. Network Pharmacology, 4(3-4), 6-30.

Bisaccia, M., Berini, F., Marinelli, F., & Binda, E. (2025). Emerging Trends in Antimicrobial Resistance in Polar Aquatic Ecosystems. Antibiotics, 14(4), 394.

Boro, D., Chirania, M., Verma, A. K., Chettri, D., & Verma, A. K. (2025). Comprehensive approaches to managing emerging contaminants in wastewater: Identification, sources, monitoring and remediation. Environmental Monitoring and Assessment, 197(4), 1-29.

Chang, T.-L. (2020). In-Situ Formation of Metal/Alloy Nanoparticles and Characterization. Stevens Institute of Technology.

Chen, Y., Yang, J., Zeng, L., & Zhu, M. (2022). Recent progress on the removal of antibiotic pollutants using photocatalytic oxidation process. Critical Reviews in Environmental Science and Technology, 52(8), 1401-1448.

Gopal, K., Tripathy, S. S., Bersillon, J. L., & Dubey, S. P. (2007). Chlorination byproducts, their toxicodynamics and removal from drinking water. Journal of hazardous materials, 140(1-2), 1-6.

Habeche, F., Boukoussa, B., Issam, I., Mokhtar, A., Lu, X., Iqbal, J., Hacini, S., Hachemaoui, M., Bengueddach, A., & Hamacha, R. (2023). Catalytic reduction of organic pollutants, antibacterial and antifungal activities of AgNPs@ CuO nanoparticles–loaded mesoporous silica. Environmental Science and Pollution Research, 30(11), 30855-30873.

Hao, Z., Wang, M., Cheng, L., Si, M., Feng, Z., & Feng, Z. (2024). Synergistic antibacterial mechanism of silver-copper bimetallic nanoparticles. Frontiers in Bioengineering and Biotechnology, 11, 1337543.

Hayyan, M., Hashim, M. A., & AlNashef, I. M. (2016). Superoxide ion: generation and chemical implications. Chemical reviews, 116(5), 3029-3085.

Ismail, M., Khan, M., Khan, S. A., Qayum, M., Khan, M. A., Anwar, Y., Akhtar, K., Asiri, A. M., & Khan, S. B. (2018). Green synthesis of antibacterial bimetallic Ag–Cu nanoparticles for catalytic reduction of persistent organic pollutants. Journal of Materials Science: Materials in Electronics, 29(24), 20840-20855.

Kankala, R. K., Han, Y. H., Na, J., Lee, C. H., Sun, Z., Wang, S. B., Kimura, T., Ok, Y. S., Yamauchi, Y., & Chen, A. Z. (2020). Nanoarchitectured structure and surface biofunctionality of mesoporous silica nanoparticles. Advanced materials, 32(23), 1907035.

Kankala, R. K., Zhang, H., Liu, C. G., Kanubaddi, K. R., Lee, C. H., Wang, S. B., Cui, W., Santos, H. A., Lin, K., & Chen, A. Z. (2019). Metal species–encapsulated mesoporous silica nanoparticles: current advancements and latest breakthroughs. Advanced functional materials, 29(43), 1902652.

Li, S., Cai, J., Wu, X., & Zheng, F. (2018). Sandwich-like TiO2@ ZnO-based noble metal (Ag, Au, Pt, or Pd) for better photo-oxidation performance: Synergistic effect between noble metal and metal oxide phases. Applied Surface Science, 443, 603-612.

Li, Z., Hou, B., Xu, Y., Wu, D., Sun, Y., Hu, W., & Deng, F. (2005). Comparative study of sol–gel-hydrothermal and sol–gel synthesis of titania–silica composite nanoparticles. Journal of Solid State Chemistry, 178(5), 1395-1405.

Lupano, L. V. L., Martínez, J. M. L., Piehl, L. L., de Celis, E. R., & Dall'Orto, V. C. (2013). Activation of H2O2 and superoxide production using a novel cobalt complex based on a polyampholyte. Applied Catalysis A: General, 467, 342-354.

Ma, L., Cai, Q., Ong, S. L., Yang, Z., Zhao, W., Duan, J., & Hu, J. (2023). Photonic efficiency optimization-oriented dependence model of characteristic coupling spectrum on catalytic absorbance in photocatalytic degradation of tetracycline hydrochloride. Chemical Engineering Journal, 451, 138623.

Muteeb, G., Rehman, M. T., Shahwan, M., & Aatif, M. (2023). Origin of antibiotics and antibiotic resistance, and their impacts on drug development: A narrative review. Pharmaceuticals, 16(11), 1615.

Phillips, L. F. (1992). Rate constants of reactions with no activation energy. Progress in energy and combustion science, 18(1), 75-90.

Salam, M. A., Al-Amin, M. Y., Salam, M. T., Pawar, J. S., Akhter, N., Rabaan, A. A., & Alqumber, M. A. (2023). Antimicrobial resistance: a growing serious threat for global public health. Healthcare,

Sangamnere, R., Misra, T., Bherwani, H., Kapley, A., & Kumar, R. (2023). A critical review of conventional and emerging wastewater treatment technologies. Sustainable Water Resources Management, 9(2), 58.

Saran, S., Manjari, G., & Devipriya, S. P. (2018). Synergistic eminently active catalytic and recyclable Ag, Cu and Ag-Cu alloy nanoparticles supported on TiO2 for sustainable and cleaner environmental applications: A phytogenic mediated synthesis. Journal of Cleaner Production, 177, 134-143.

Sarina, S., Waclawik, E. R., & Zhu, H. (2013). Photocatalysis on supported gold and silver nanoparticles under ultraviolet and visible light irradiation. Green Chemistry, 15(7), 1814-1833.

Shchukin, D. G., & Sviridov, D. V. (2006). Photocatalytic processes in spatially confined micro-and nanoreactors. Journal of Photochemistry and Photobiology C: Photochemistry Reviews, 7(1), 23-39.

Sun, P., Cheng, L., Gao, S., Weng, X., & Dong, X. (2023). Industrial chlorinated organic removal with elimination of secondary pollution: a perspective. The Journal of Physical Chemistry C, 127(14), 6610-6618.

Tantawy, H. R., Nada, A. A., Baraka, A., & Elsayed, M. A. (2021). Novel synthesis of bimetallic Ag-Cu nanocatalysts for rapid oxidative and reductive degradation of anionic and cationic dyes. Applied Surface Science Advances, 3, 100056.

Umar, M. (2022). From conventional disinfection to antibiotic resistance control—Status of the use of chlorine and UV irradiation during wastewater treatment. International Journal of Environmental Research and Public Health, 19(3), 1636.

Wang, F., Xiang, L., Sze-Yin Leung, K., Elsner, M., Zhang, Y., Guo, Y., Pan, B., Sun, H., An, T., & Ying, G. (2024). Emerging contaminants: A One Health perspective. The Innovation 5 (4), 100612. In: REVIEW.

Xie, Z.-H., He, C.-S., Zhou, H.-Y., Li, L.-L., Liu, Y., Du, Y., Liu, W., Mu, Y., & Lai, B. (2022). Effects of molecular structure on organic contaminants' degradation efficiency and dominant ROS in the advanced oxidation process with multiple ROS. Environmental Science & Technology, 56(12), 8784-8795.

Zhang, Y., Ma, D., Li, J., Chen, Y., Shi, L., Feng, X., & Shi, J.-W. (2025). Confinement effects in photocatalysis: progress and challenges. Journal of Materials Chemistry A, 13(15), 10431-10450.

Zhang, Z., Du, F., Shi, H., Du, H., & Xiao, P. (2025). Iron Redox Cycling in Persulfate Activation: Strategic Enhancements, Mechanistic Insights, and Environmental Applications—A Review. Nanomaterials, 15(22), 1712.